A New Measurement-Based Algorithm for the Temporal Resolution of the Clear-Sky Solar Resource

P.A. Perumall[a], J.P. Pitot de la Beaujardiere[b], M.J. Brooks[c]

Received 24 June 2014, in revised form 17 August 2015 and accepted 4 September 2015

Abstract ***For any solar concentrator system, a thorough understanding of daily and seasonal variations of direct normal irradiance (DNI) under clear-sky conditions is required. This paper presents an algorithm which processes historical ground-based solar measurements to generate a continuous function that estimates clear-sky DNI magnitude as a function of solar time and day number over a typical year. The three-dimensional surface that results from this function is termed a Temporal DNI Topograph (TDT) and can be used to define solar flux input for the modelling of concentrator systems. TDTs developed for Durban and Stellenbosch (South Africa) are presented and statistically compared to clear-sky DNI approximations of four simple radiative models. It is concluded that the Fu Rich, ASHRAE and Kumar radiative models are suitable for use in initial system design and performance studies. In addition, revised bulk atmospheric transmittance values are proposed for the implementation of the Fu Rich model at Durban and Stellenbosch, based upon comparisons to the TDT predictions.***

Additional keywords: Clear-sky DNI, solar furnace, CSP.

1 Introduction

The performance of systems that employ solar concentrators, such as concentrating solar power (CSP) plants, is commonly assessed over a year-long period on the basis of radiometric and meteorological data that are representative of typical, site-specific conditions. Typical meteorological year (TMY) data files are, for example, a source of such data.

In any solar concentration system the beam component of solar radiation, commonly referred to as direct normal irradiance (DNI), provides the primary input to system performance analyses. For accurate estimation of energy outputs, the impact of diurnal, seasonal and meteorological variations on DNI needs to be captured. The DNI data considered in annual analyses can therefore be termed "all-sky" DNI data, as DNI records associated with both clear and cloudy days are used to calculate the expected energy yield of the system.

On the other hand, "clear-sky" DNI data is a subset of all-sky DNI data that is exclusively associated with cloudless conditions. Although clear-sky DNI data are not in themselves sufficient to predict annual system performance, they are of particular importance in the design of solar concentrator systems and associated equipment, as reported in the literature.

Examples of the use of clear-sky DNI data abound in the literature. Bader et al. describe a model for a parabolic trough tubular cavity-receiver in which they model the clear-sky DNI for Seville, Spain, "*at the summer solstice at solar noon*" and again "*for the equinox at 8 am solar time*."[1] This is similar to the type of time and date-specific radiometric data produced by the algorithm proposed here. Huang et al. apply a non-empirical clear-sky DNI model to generate irradiance values in the simulation of a parabolic trough's performance.[2] Samanes and Garcia-Barberena model a cavity-type receiver and also use a set of clear-sky DNI curves as inputs to their simulation.[3] In the absence of a clear-sky DNI prediction model they selected a run of five clean daily profiles from a Baseline Surface Radiation Network ground station in Nevada, USA, to use as the DNI input. Yilmaz and Söylemez describe a parabolic trough collector model that uses as its energy input "*a typical beam radiation measured in the summer solstice for Gaziantep (Turkey)*".[4] Once again, their DNI input is a clear-sky profile.

Apart from simulation studies, knowledge of site-specific clear-sky DNI is also required during the planning and execution phases of a concentrator test programme. A practical problem that arises is structuring the test programme such that reasonable baseline DNI is available throughout the testing window at a given location, accounting for daily and seasonal variability, but excluding cloud effects. Standards such as ASHRAE[5] and EN 12975[6] stipulate irradiance levels required during collector evaluation, so knowledge of the clear-sky DNI is essential. For example, Brooks used a solar position algorithm to generate a graph of incidence angles covering the period of a parabolic trough test programme in Durban.[7]

The present study has been undertaken in support of the University of KwaZulu-Natal's Solar Energy Research Amplified Flux Facility (SERAFF) project[8], which seeks to develop South Africa's first dedicated solar furnace research facility.

Solar furnaces typically operate under clear-sky conditions, where high DNI and minimal radiation interruptions are desired. To appropriately schedule test campaigns it is therefore important to be able to forecast the clear-sky DNI resource available at the facility's location at any time during the year. This is since the diurnal and seasonal variation of this parameter impacts directly upon the nature of and duration over which testing can be conducted in the context of minimum threshold values.

An established approach to provide such forecasts is the use of clear-sky radiative models which estimate clear-sky

a. Graduate Student, Discipline of Mechanical Engineering, University of KwaZulu-Natal, Durban.
b. Lecturer, Discipline of Mechanical Engineering, University of KwaZulu-Natal, Durban, e-mail: pitot@ukzn.ac.za.
c. Member SAIMechE, Senior Lecturer, Discipline of Mechanical Engineering, University of KwaZulu-Natal, Durban.

DNI as a function of time and location, based upon attenuation parameters. Whilst these models are quite simple and are not generally reliant upon ground-based measurements, the uncertainty associated with their predictions is typically high. For high-fidelity system design and performance calculations, this level of uncertainty is not desirable.

In this study we consider the problem of processing and presenting 1-minute radiometric data from ground stations so that they can be more usefully integrated in concentrator system performance models. In particular, the development of a novel algorithm for formulating a continuous function describing the daily and seasonal variation of clear-sky DNI based on such data is detailed. The three-dimensional surface that results is termed a temporal DNI topograph (TDT).

The algorithm is implemented to derive TDT models for Durban and Stellenbosch, and the value of the information revealed by these models is illustrated in the specific context of considerations associated with solar furnace operation. In addition, the TDT results derived above are compared on a statistical basis to predictions made by a variety of clear-sky radiative models, allowing the fidelity and applicability of these models to be evaluated. Finally, the effectiveness of using TDT models to tune the attenuation parameters of one such radiative model in order to enhance its prediction accuracy is also demonstrated.

2 Methodology

2.1 Measurement of DNI

The temporal DNI topographs presented here were obtained from measurements of down-welling short-wave irradiance taken by instruments located at two ground stations. The Durban station is located at the University of KwaZulu-Natal's Howard College campus and includes an Eppley Laboratory Normal Incidence Pyrheliometer (NIP) (serial # 35649E6) and a Kipp & Zonen CHP1 pyrheliometer (serial # 120791) for DNI measurement. The NIP is an ISO 9060 secondary standard instrument with measurement uncertainty of approximately 1.5 to 2%. The CHP1 exhibits similar but slightly lower uncertainties. Most of the Durban data used in this study were obtained from the GRADRAD archive[9]. The Stellenbosch data were measured using a Kipp & Zonen CHP1 (Serial # 100235) and downloaded from the SAURAN website[10]. Data used in the study were recorded as minute averaged values between 2010 and 2013 at both sites. In figure 1 the data process flow for the study is given. Blocks (A) to (D) illustrate the steps followed in acquiring and preparing the raw DNI data. Blocks (E) to (G) represent the processing required to generate the temporal DNI topographs.

2.2 Extraction of Clear-Sky Days

Block (E) of figure 1 represents a screening process in which the raw DNI data files for each day are categorized as either clear or cloudy days. The filtering process was done by visual inspection of DNI as a function of solar time for each day. Clear-sky days exhibit the typical profile shown in red in figure 2. Partly cloudy days produce stochastic variation in the data trace, as shown in blue in figure 2. Although visual inspection is somewhat subjective, it is commonly used in radiometric studies[11] and was applied here to isolate days with radiometric profiles similar to that of the clear-sky day in figure 2.

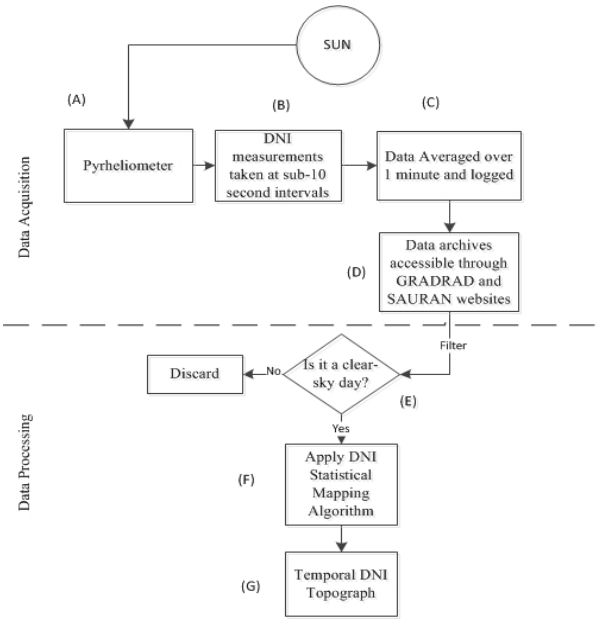


Figure 1: Overview of DNI measurement data flow.

Once the database of clear-sky days was formed, the more complex task of transforming the measurements into a useful representation of sun strength spanning a full calendar-year was undertaken, as described in section 2.3.

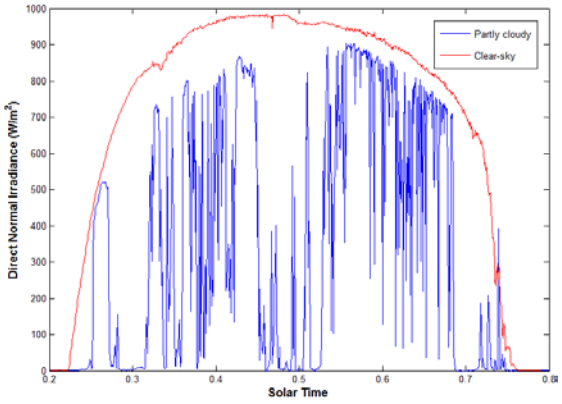


Figure 2: Comparative traces of DNI measured under clear and partly cloudy sky conditions at Durban.

2.3 Temporal DNI Topograph Mapping Algorithm

The intention of this study was to utilize high frequency DNI measurements in order to build a map correlating clear-sky DNI magnitude with daily and seasonal changes with time. The multivariate approach results in a three-dimensional surface or topograph of DNI that excludes partly cloudy conditions.

The number of cloud-free days in the dataset is naturally limited by the influence of weather conditions. In total, 59 clear-sky days were used for the Durban station's analysis spanning all 12 months of a generic year. This number was

increased to 96 for Stellenbosch where weather conditions result in more frequent cloud-free conditions.

The manipulation of data was undertaken using matrix-algebra, as follows. Twelve matrices were generated, one for each month (D_{month}) of a generic year. Each consists of raw, minute-averaged values of clear-sky DNI running from 08:00 to 16:00 (solar time), that is from solar minute 480 to solar minute 960. The time period is consistent with the practical daily operating window of a specialized concentrating system, such as the solar furnace. The column entries represent all available clear-sky day numbers from 1 to a maximum of C in a particular month. This utilized all data, that is, January measurements from 2010 to 2013, all February measurements from 2010 to 2013, and so on up to and including December.

$$D_{month} = \begin{Bmatrix} a_{480,1} & \cdots & a_{480,C} \\ \vdots & \ddots & \vdots \\ a_{960,1} & \cdots & a_{960,C} \end{Bmatrix} \quad (a)$$

Once matrix (a) is constructed for the 12 months of the year a second matrix is generated (b) to represent the average DNI per minute for all clear-sky days in a particular month. In essence, this is the average measured clear-sky DNI for a particular month as a function of solar time.

$$D_{monthly_Average} = \begin{Bmatrix} b_{n,1} \\ \vdots \\ b_{481,1} \end{Bmatrix} \quad (b)$$

Element $b_{n,1}$ is given by equation (1), noting that $n \in (1{:}\,481)$ where $n = 1$ corresponds to 8:00AM and n = 481 corresponds to 16:00PM.

$$b_{n,1} = \frac{\sum_{i=1}^{C} (a_{n,i} + a_{n,i+1} + a_{n,i+2} + \cdots + a_{n,C})}{C} \quad (1)$$

A 6th order polynomial was used to curve fit the average clear-sky DNI plots for each month. A set of twelve polynomial equations are thus formed which represent the average clear sky DNI profile (DNI_{minute}) as a function of solar minute for each of the 12 months of the generic year. Equation (2) is the general form of these equations:

$$DNI_{minute} = p_1 m^6 + p_2 m^5 + p_3 m^4 + p_4 m^3 + p_5 m^2 + p_6 m + p_7 \quad (2)$$

where m is the solar time in minutes, m = 1 corresponds to 08:00 and p_1 to p_7 are the polynomial coefficients.

These 12 equations are assembled around the mean day number of that month to achieve an unbiased average clear-sky DNI per minute for that month.

The MATLAB software package is used to interpolate between the 12 equations using a 6th order polynomial. This produces a new set of equations of the form given below, that approximate clear-sky DNI explicitly as a function of day number (N) and implicitly as a function of solar time.

$$DNI = q_1 N^6 + q_2 N^5 + q_3 N^4 + q_4 N^3 + q_5 N^2 + q_6 N + q_7 \quad (3)$$

These equations are used to generate the TDT.

2.4 Temporal DNI Topograph (TDT)

The mapping algorithm is used to generate the TDT showing both seasonal and daily variations in clear-sky DNI. Figures 3 and 4 give the resulting temporal DNI topographs for Durban and Stellenbosch respectively.

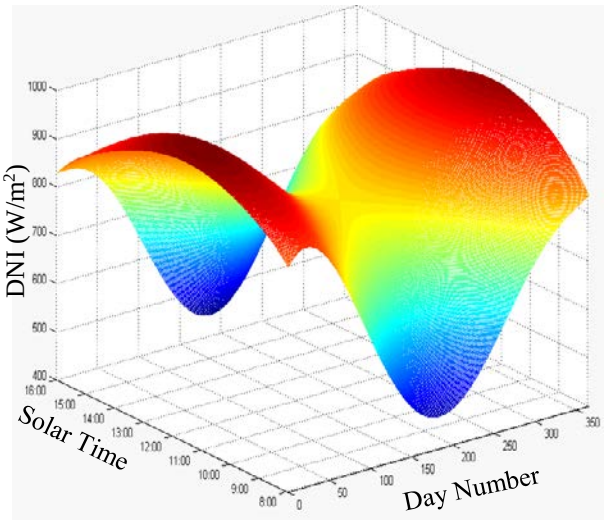


Figure 3: Temporal DNI topograph for Durban.

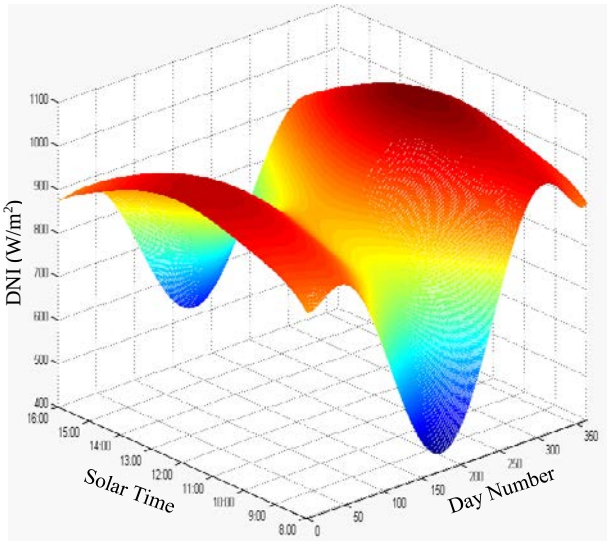


Figure 4: Temporal DNI topograph for Stellenbosch.

It can be seen that Stellenbosch receives, on average, higher levels of clear-sky DNI throughout the year. This is consistent with the type of weather patterns experienced at the two sites. As expected, both receive maximum clear-sky DNI in summer and minimum levels in winter as indicated by the depression in the saddle-shaped TDT. With minimal further analysis, the map can be used to identify the range of days throughout the year in which a solar furnace or any concentrating solar equipment can be run if a minimum DNI threshold must be exceeded. This is not possible with spatial or annually averaged all-sky DNI maps, nor is it easily achievable using data from conventional solar resource assessment studies. As well as being able to observe the seasonal variations, the map allows the observation of daily variability which is useful in gauging an optimum window of operation for solar concentrators. Cross sections of the map illustrate the usefulness of the TDT in identifying solar irradiance trends and limits, as shown in figures 5 and 6.

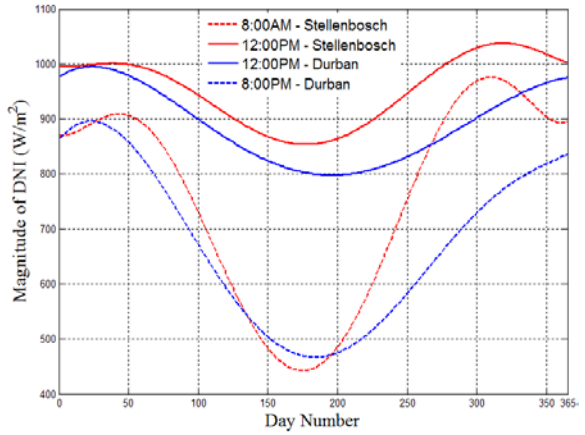


Figure 5: TDT cross-section for 08:00 and 12:00 at Durban and Stellenbosch showing seasonal variation

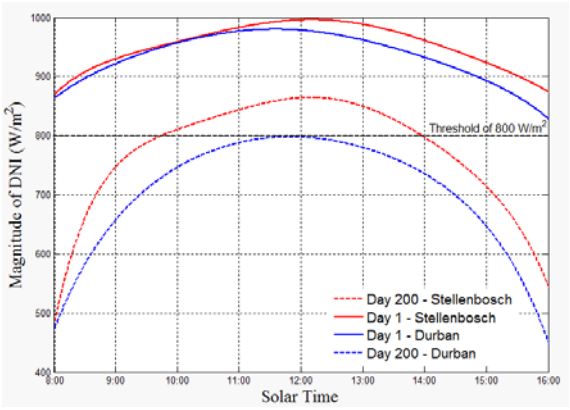


Figure 6: TDT cross-section taken for Day 1 (summer) and Day 200 (winter) for Durban and Stellenbosch showing daily variation.

Among other trends, figure 6 shows the steeper seasonal gradient in clear-sky DNI at 08:00 for both Durban and Stellenbosch versus that at 12:00. This illustrates the reduced operational window for the SERAFF solar furnace which must be operated nearer to solar noon as winter approaches, for the hypothetical case of an 800 W/m^2 flux threshold. Summer offers the opportunity for an earlier start in the morning. Figure 6 gives the daily variation for Day 1 (summer day) and Day 200 (winter Day). In early January there are more hours available in which to run SERAFF, with respect to the flux threshold, as compared to Day 200 where there are fewer hours available that meet or exceed this threshold. In the case of Durban for Day 200, it is unlikely that SERAFF would achieve the thermal flux corresponding to the hypothetical DNI threshold at any time of the day.

Apart from inspecting cross-sections of the TDT, a more powerful application would be to use the individual clear-sky DNI points, which make up the mapped surface, as inputs to an optical system model. This can be a model simulating the optical behaviour of any specialized solar concentrating equipment that harnesses DNI.

In this case, the TDT can be directly applied to the design of a solar furnace such as SERAFF. For instance, it would prove useful to apply the temporal map to an optical model of the heliostat, where the total collected aperture irradiation over the course of a day is to be considered, specifically during the window of operation.

For information purposes, the underlying TDT data for Durban and Stellenbosch are available on request from the authors.

2.5 Clear-Sky Radiative Models

In the absence of ground-based radiometric measurements, solar energy design engineers may use one of the many clear-sky radiative models to estimate the local solar resource[12]. These are time and location-dependent and can therefore provide the estimated energy input to solar concentrator performance analyses for different sites. An obvious drawback is that they carry uncertainties versus reference data that compromise the equipment performance models to which they are applied. In some cases, a radiometric model may need to be tuned to a specific site to improve its accuracy. Four such models are therefore included in this study to illustrate the improvement in clear-sky DNI prediction that might be expected from the empirically derived TDT.

The most accurate clear sky models are based on the attenuation of solar radiation by scattering and absorption as sunlight traverses the atmosphere to ground[13]. Their statistical uncertainty is therefore related to their complexity and generally also to the number of inputs to the model. As an example of the general form, Bird and Hulstrom[13] proposed the following model of beam irradiance:

$$\mathrm{DNI} = E_0 \cdot 0.9662 \cdot T_r \cdot T_a \cdot T_w \cdot T_0 \cdot T_u \qquad (4)$$

Here T_r, T_a, T_w, T_0 and T_u are transmittance factors that describe Rayleigh scattering, aerosol absorptance/scattering, water vapour absorption, ozone absorption and uniformly mixed gas absorption, respectively. E_0 is the extraterrestrial irradiance at the mean earth-sun distance. These factors are not easily obtained for a site without a ground-based measurement station and their use in concentrator performance modelling and design is therefore problematic. Simpler models eliminate the problem and there are several in common use

2.6 Selected Radiative Models

Four clear-sky models that require fewer measured inputs than the attenuation variety are those of ASHRAE[5], Fu and Rich[14], Hottel[15], and Kumar[16].

In this study, these models are applied to estimate clear-sky DNI for Durban and Stellenbosch for comparison with the TDT maps presented in this paper. As a spin-off from the current work, the model proposed by Fu and Rich[14] is tuned to local conditions so that it more accurately represents the clear-sky DNI resource for Durban and Stellenbosch. This includes adjusting the bulk atmospheric transmittance parameter as determined by the TDT analysis.

The chosen models require few or no atmospheric inputs. Their primary input variable is the solar zenith angle which, for the present study, was obtained at 1-minute intervals for the period of 2010 to 2013, using the US National Renewable Energy Laboratory (NREL) Solar Position Algorithm[17]

2.6.1 ASHRAE Model

The ASHRAE model is used in industry to calculate solar heat gains and cooling loads in buildings and in the design of simple solar systems. It is a simple decaying function that is independent of atmospheric data. It is a function of the solar zenith angle, *Z*. Clear-sky DNI is obtained from:

$$DNI = A_m e^{(\frac{-B_m}{\cos Z})} \quad (5)$$

where A_m and B_m are fixed monthly coefficients that are determined empirically[5].

2.6.2 Hottel Model

The model of Hottel[15] has been successfully utilized in estimating clear-sky solar irradiances for sites around the world[18, 19]. The direct component is obtained from:

$$DNI = E_0(a_0 + a_1 \cdot e^{-k.\sec Z}) \quad (6)$$

The constants in parenthesis are collectively regarded as an atmospheric transmittance factor, where constants a_0, a_1 and k are calculated using the following equations based on the urban 5 km visibility haze model.

$$a_0 = 0.4237 - 0.00821(6 - A)^2 \quad (7a)$$

$$a_1 = 0.5055 + 0.00595(6.5 - A)^2 \quad (7b)$$

$$k = 0.2711 + 0.01858(2.5 - A)^2 \quad (7c)$$

The atmospheric transmittance constants are functions of site altitude, *A*, only. E_0 is the extra-terrestrial irradiance given by:

$$E_0 = 1367.(\frac{R_{av}}{R})^2 \quad (8)$$

The ratio R_{av}/R is the ratio of mean sun-earth distance to the actual sun-earth distance as a function of the day number (*N*) of the year. This ratio is obtained from the Fourier series representation of the sun's position given by Spencer[20].

2.6.3 Kumar Model

The model proposed by Kumar[16] has been used in the agricultural and ecology sectors to estimate solar irradiance[21]. Clear-sky DNI is obtained as follows:

$$DNI = 0.56.E_0.(e^{-0.65.m_k} + e^{-0.095.m_k}) \quad (9)$$

where the term m_k is given by:

$$m_k = \left(\frac{p}{p_0}\right)[(1229 + (614\cos Z)^2)^{0.5} 614\cos Z) \quad (10)$$

The term m_k is a function of the solar zenith angle and the ratio of local barometric pressure to standard pressure at sea level, p/p_0. This ratio is set to unity because Durban and Stellenbosch are situated close to sea level. As a check on this assumption, model sensitivity was tested by applying a variable pressure ratio to equation (10), based on meteorological data for multiple clear-sky days. The resulting clear-sky DNI estimations were shown to exhibit no significant difference as compared to approximations with an assumed pressure ratio of 1.

2.6.4 Fu and Rich Model

The clear-sky model proposed by Fu and Rich[14] was developed for Geographic Information Systems (GIS) applications. The model requires only solar zenith angle and site elevation. Clear-sky DNI is obtained from:

$$DNI = E_0.{T_b}^{m_f} \quad (11)$$

where T_b is the bulk atmospheric transmittance factor with recommended value of 0.5 and air mass factor given by:

$$m_f = \frac{e^{(-0.000118.h - 1.638x10^{-9}.h^2)}}{\cos Z} \quad (12)$$

The air mass factor is a function of solar zenith angle and the site elevation, *h* in meters.

2.7 Three-Dimensional DNI Temporal Map based on Radiative Model DNI Approximations

In this section, the DNI topographs derived from pyrheliometric measurement are compared to similar surfaces generated using artificial clear-sky DNI data from the radiative models. This is useful in highlighting the models' failure to capture physical trends in the local solar resource, versus the empirically-based TDTs. Figures 7 and 8 show individual maps generated using the models mentioned, as well as the TDT illustrated in section 2.4.

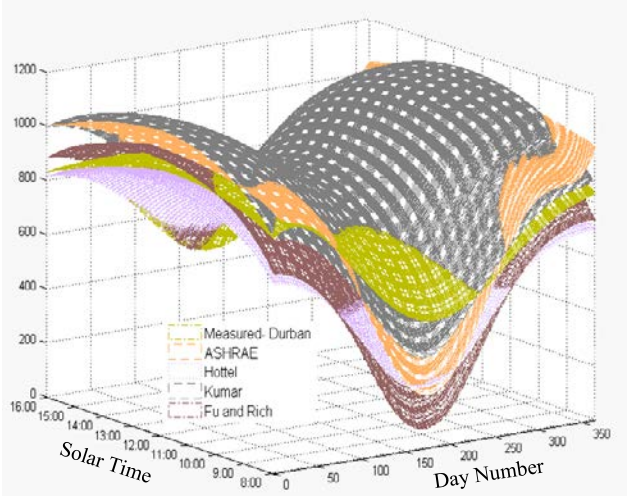


Figure 7: Comparison of model-generated surfaces and the empirically derived TDT for Durban.

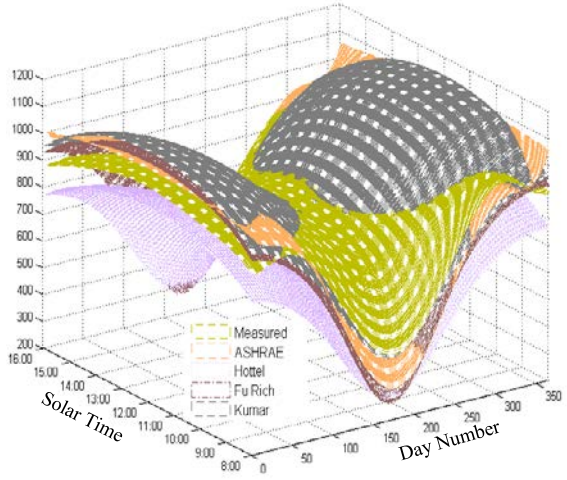


Figure 8: Comparison of model-generated surfaces and the empirically derived TDT for Stellenbosch.

Upon visual inspection, the modelled maps and measured maps show fairly tight grouping and in some instances overlap one another. The general 'saddle' shape is exhibited for all instances of the modelled maps.

2.8 Mean Bias Error (MBE) and Root Mean Square Error (RMSE)

The differences between the modelled and measured maps are quantified statistically using the mean bias difference (MBD) and the root mean square difference (RMSD). Table 1 gives the cumulative RMSD and MBD values, expressed as a percentage of the mean measured irradiance in W/m^2, and derived as follows:

$$\text{MBD} = \frac{\sum_{i=1}^{k}(DNI_{model,i} - DNI_{measured,i})}{k} \quad (13)$$

$$\text{RMSD} = \sqrt{\frac{\sum_{i=1}^{k}(DNI_{model,i} - DNI_{measured,i})^2}{k}} \quad (14)$$

where DNI_{model} and $DNI_{measured}$ are the model approximated and measured clear-sky DNI magnitudes for each interval (i), respectively. The variable k represents the total number of data points used in the calculation, for example k = 365 and k =480 for a seasonal (per day) and daily (per minute) analysis, respectively.

Table 1: Annual cumulative MBD and RMSD statistics for Durban and Stellenbosch.

#	Model	Durban		Stellenbosch	
		MBD (%)	RMSD (%)	MBD (%)	RMSD (%)
1	ASHRAE	+6.8	9.8	-2.7	8.1
2	Hottel	-6.5	8.1	-15.9	16.9
3	Kumar	+13.8	15.3	+3.2	6.7
4	Fu Rich	-0.4	10.2	-0.3	6.7

The mean bias difference of model 4 is considerably lower than those of models 1, 2 and 3 for Durban and Stellenbosch as the model was tuned to these specific locations against the measured TDT. The bulk atmospheric transmittance factor (T_b) cannot be determined independently of atmospheric data therefore a recommended value of 0.5 is given in the literature[22]. The MBD based on the entire dataset, for model 4, is minimized such that it approaches zero as the bulk atmospheric transmittance factor goes to unity. It was found that the recommended value of T_b for both Durban and Stellenbosch is 0.72 and 0.77, respectively.

Models 1 and 2 perform similarly for Durban, but largely differ for Stellenbosch. This could be due to Model 2's dependence on the Haze model of equation (7) where the various atmospheric parameters are approximated.

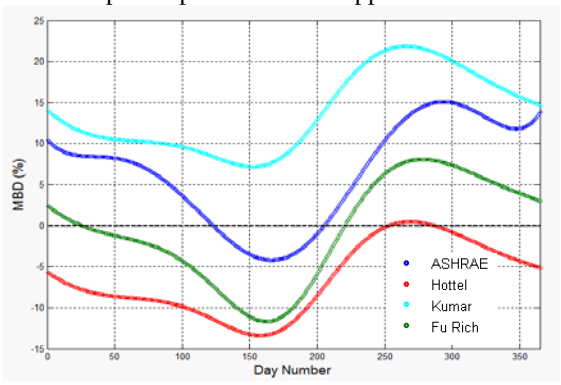


Figure 9: MBD as a percentage of mean measured clear-sky DNI per day for Durban.

Although the cumulative statistics indicate a measure of error over the entire dataset, it is instructive to investigate the performance of the models at each minute and over an entire day. These statistics appear in figures 9 to 16.

A solar furnace is typically operated within an available period of time in order to successfully conduct an experiment or testing procedure. Therefore in applying a model to predict clear-sky DNI in the absence of ground-based measurements it is critical to gauge the performance of the models on a minutely and daily basis.

All models underestimate clear-sky DNI throughout winter and tend to overestimate it in summer. Certainly this is suggestive of the incapability of these simple radiative models to accurately predict seasonal variations in clear-sky DNI. However, the models ASHRAE, Kumar and the tuned Fu Rich models, perform well with minutely approximations of clear-sky DNI for both Durban and Stellenbosch. These models exhibit fairly constant bias and RMSD for approximately 75% of the day. All four models become inaccurate during early morning periods and towards late afternoon. This can be due to the fact that these models do not require atmospheric data; therefore modification cannot be made to account for factors such as high levels of particulate matter in the air.

The ASHRAE and tuned Fu Rich models tend to be the most stable and suitably accurate per minute approximations of clear-sky DNI in the absence of ground-based measurements. This capability lends itself well to initial studies concerning the design of solar concentrating equipment.

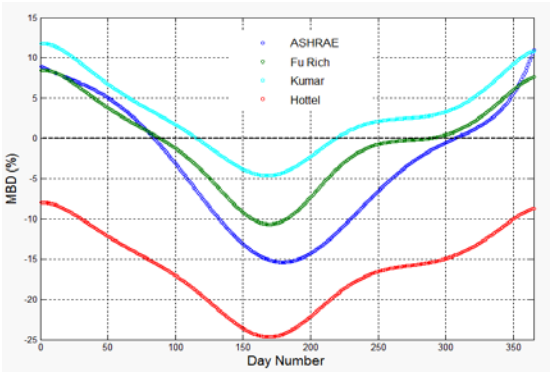


Figure 10: MBD as a percentage of mean measured clear-sky DNI per day for Stellenbosch.

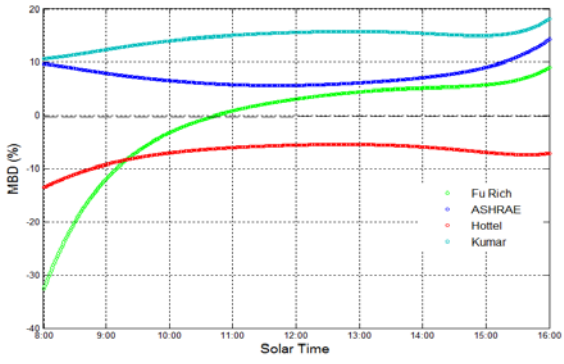


Figure 11: MBD as a percentage of mean measured clear-sky DNI per minute for Durban.

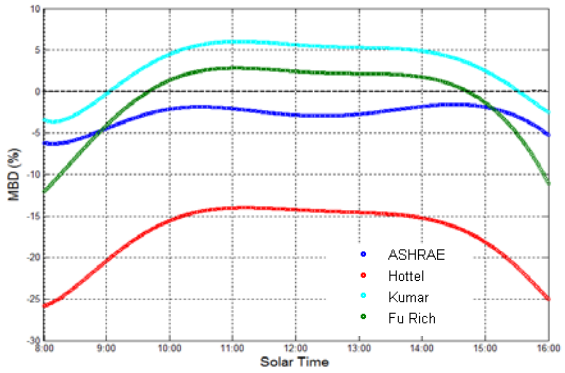


Figure 12: MBD as a percentage of mean measured clear-sky DNI per minute for Stellenbosch.

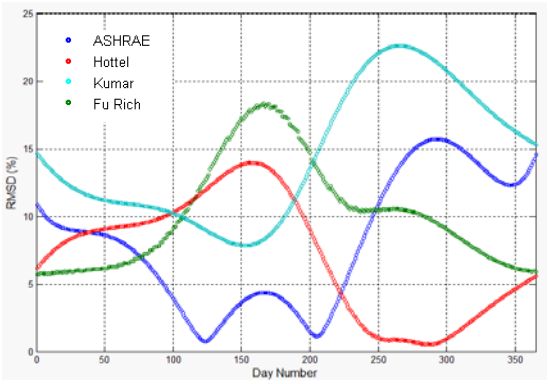


Figure 13: RMSD as a percentage of mean measured clear-sky DNI per day for Durban.

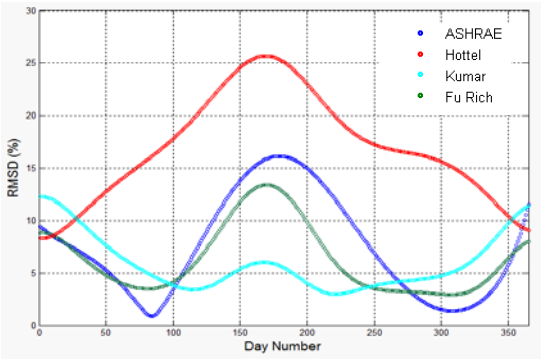


Figure 14: RMSD as a percentage of mean measured clear-sky DNI per day for Stellenbosch.

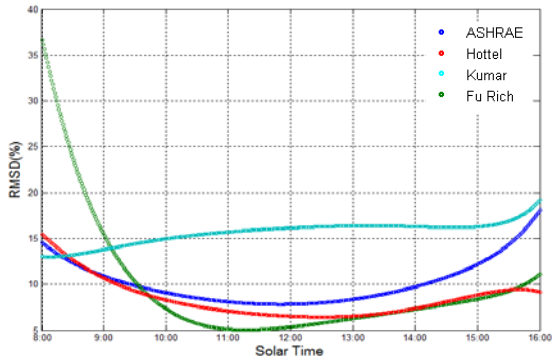


Figure 15: RMSD as a percentage of mean measured clear-sky DNI per minute for Durban.

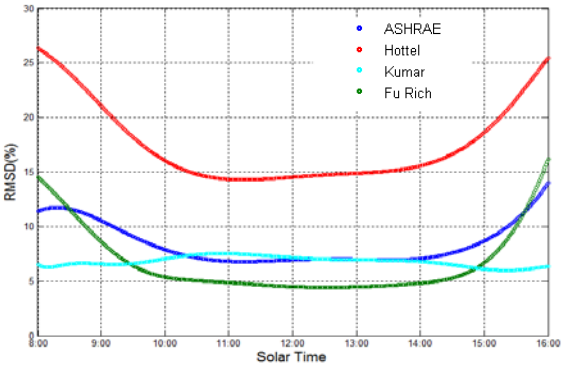


Figure 16: RMSD as a percentage of mean measured clear-sky DNI per minute for Stellenbosch.

3 Conclusion

The development and implementation of a novel algorithm for the formulation of a measurement-based model that can predict the daily and seasonal variation of clear-sky DNI at a specific location has been detailed.

The three-dimensional surface generated by the model – termed a temporal DNI topograph (TDT) – reveals seasonal variations in clear-sky DNI as well as daily variability. Although it excludes the effect of opaque cloud, the model includes the effect of other attenuation sources such as site-specific, seasonal pollution phenomena. It can thus indicate the temporal and seasonal limits that bound operating windows associated with solar concentrator systems such as solar furnaces, where the clear-sky DNI must exceed a particular threshold value. This is achieved more accurately than through the use of clear-sky radiative models in which clear-sky DNI is modelled primarily as a function of air mass.

Since the empirically-derived TDT offers an alternative prediction capability to clear-sky models, four such models were used to generate comparative maps for Durban and Stellenbosch. A statistical analysis showed that the ASHRAE and tuned Fu Rich models performed best when approximating clear-sky DNI on a daily per-minute basis, estimating values within ±5% for Stellenbosch and ±10% for Durban. However, the same models did not perform as well in predicting seasonal variations of clear-sky DNI, underestimating values by as much as 25% in winter. With the aid of the measurement-based TDT, the above radiative models have been shown to be reasonable for use in preliminary solar concentrating equipment design studies at sites where there is an absence of ground-based measurements.

An exhaustive comparison of the TDT with ground measurements of clear-sky DNI is necessary to further quantify the uncertainties associated with the TDT modelling approach. This will become possible as the clear sky datasets for Durban and Stellenbosch are expanded over time and inter-annual variability in the underlying measurements is better understood. In addition, it may be possible to increase the input data to the TDT algorithm by incorporating clear-sky trace segments from otherwise partly cloudy days. This would augment the underlying data, but the filtering process for selecting such measurements may require a more robust approach than the visual method used here. These issues may be addressed in future studies.

 © SAIMechE All rights reserved.

Acknowledgements

The authors are grateful to Prof. Graham Smith for his input. This research was supported and funded by the National Research Foundation of South Africa and the Eskom TESP Programme.

References

1. *Bader R, Pedretti A, Barbato M* and *Steinfeld A*, An Air-based Corrugated Cavity-receiver for Solar Parabolic Trough Concentrators, *Applied Energy*, 138, 337–345, 2015.
2. *Huang W, Hu P* and *Chen Z*, Performance Simulation of a Parabolic Trough Solar Collector, *Solar Energy*, 86 (2), 746–755, 2012.
3. *Samanes J* and *Garcia-Barberena J*, A Model for the Transient Performance Simulation of Solar Cavity Receivers, *Solar Energy*, 110, 789–806, 2014.
4. *Yilmaz IH* and *Söylemez MS*, Thermo-mathematical Modeling of Parabolic Trough Collector, *Energy Conversion and Management*, 88, 768–784, 2014.
5. ASHRAE, Handbook of Fundamentals. American Society of Heating, Refrigeration and Air-Conditioning Engineers Inc., 1972.
6. BS EN 12975-1: Thermal Solar Systems and Components - Solar Collectors, British Standard, 2006.
7. *Brooks MJ*, Performance of a Parabolic Trough Solar Collector, MScEng Thesis, Stellenbosch University, 2005
8. *Perumall PA, Pitot J* and *Brooks MJ*, An Introduction to the University of KwaZulu-Natal's Solar Energy Research Amplified Flux Facility, *Proceedings of the 13th International Energy Conversion Engineering Conference*, 2015.
9. *Kunene KR, Brooks MJ, Roberts LW* and *Zawilska E*, Introducing GRADRAD: The Greater Durban Radiometric Network, *Renewable Energy*, 49, 259-262, 2013.
10. SAURAN. Southern African Universities Radiometric Network, www.sauran.net, 2014.
11. *Salazar GA* and *Raichijk C*, Evaluation of Clear-sky Conditions in High Altitude Sites, *Renewable Energy*, 64, 197-202, 2014.
12. *Gueymard CA*, Temporal Variability in Direct and Global Irradiance at Various Time Scales as Affected by Aerosols, *Solar Energy*, 86 (12), 3544-3553, 2012.
13. *Bird RE* and *Hulstrom RL*, A Simplified Clear Sky Model for Direct and Diffuse Insolation on Horizontal Surfaces, Report No SERI/TR-642-761, Solar Energy Research Institute, Golden, CO (USA), 1981.
14. *Fu P* and *Rich P*, Design and Implementation of the Solar Analyst: an ArcView Extension for Modelling Solar Radiation at Landscape Scales, *Proceedings of the 19th Annual ESRI User Conference*, 1-31, 1999.
15. *Hottel HC*, A Simple Model for Estimating the Transmittance of Direct Solar Radiation through Clear Atmospheres, *Solar Energy*, 18 (2), 129-134, 1976.
16. *Kumar L*, Modelling Topographic Variation in Solar Radiation in a GIS Environment, *International Journal of Geographical Information Sciences*, 11 (5), 475-497, 1997.
17. SPA, Solar Position Algorithm. www.nrel.gov/midc/solpos/spa.html, 2014
18. *Lingamgunta C* and *Veziroglu TN*, A Universal Relationship for Estimating Daily Clear Sky Insolation, *Energy Conversion and Management*, 45 (15), 2313-2333, 2004.
19. *Aziz A* and *Gamil M*, Estimation of Hourly Clear-sky Solar Radiation for PDR Yemen, *Solar & Wind Technology*, 7 (2), 255-260, 1990.
20. *Spencer JW*, Fourier Series Representation of the Position of the Sun, *Search*, 2 (5), 172, 1971.
21. *Spadavecchia L, Williams M, Bell R, Stoy PC, Huntley B* and *van Wijk T*, Topographic Controls on the Leaf Area Index and Plant Functional Type of a Tundra Ecosystem, *Journal of Ecology*, 96 (6), 1238-1251, 2008.
22. *Gueymard CA*, Clear-sky Irradiance Predictions for Solar Resource Mapping and Large-scale Applications: Improved Validation Methodology and Performance Analysis of 18 Broadband Radiative Models, *Solar Energy*, 86 (8), 2145-2169, 2012.

 © SAIMechE All rights reserved.